

Estimation of Mixed-Phase Cloud Optical Depth and Position Using In Situ Radiation and Cloud Microphysical Measurements Obtained from a Tethered-Balloon Platform

M. SIKAND, J. KOSKULICS, AND K. STAMNES

Department of Physics, Stevens Institute of Technology, Hoboken, New Jersey

B. HAMRE AND J. J. STAMNES

Department of Physics and Technology, University of Bergen, Bergen, Norway

R. P. LAWSON

SPEC Incorporated, Boulder, Colorado

(Manuscript received 21 February 2012, in final form 24 July 2012)

ABSTRACT

Microphysical and radiative measurements in boundary layer mixed-phase clouds (MPCs), consisting of ice crystals and liquid droplets, have been analyzed. These cloud measurements were collected during a May–June 2008 tethered-balloon campaign in Ny-Ålesund, Norway, located at 78.9°N, 11.9°E in the High Arctic. The instruments deployed on the tethered-balloon platform included a radiometer, a cloud particle imager (CPI), and a meteorological package. To analyze the data, a radiative transfer model (RTM) was constructed with two cloud layers—consistent with the CPI data—embedded in a background Rayleigh scattering atmosphere. The mean intensities estimated from the radiometer measurements on the balloon were used in conjunction with the RTM to quantify the vertical structure of the MPC system, while the downward irradiances measured by an upward-looking ground-based radiometer were used to constrain the total cloud optical depth. The time series of radiometer and CPI data obtained while profiling the cloud system was used to estimate the time evolution of the liquid water and ice particle optical depths as well as the vertical location of the two cloud layers.

1. Introduction

Clouds are important in understanding the earth's radiation budget and climate. Mixed-phase clouds (MPCs), consisting of supercooled liquid droplets and ice crystals, have been found to cover large areas in the Arctic (Shupe 2011). MPCs tend to consist of stratiform layers of supercooled liquid water from which ice crystals form and precipitate (Curry et al. 1997; Rangno and Hobbs 2001; Shupe et al. 2006; Verlinde et al. 2007; de Boer et al. 2009; Sikand et al. 2010; Lawson et al. 2011). Even though a mixture of supercooled droplets and ice is microphysically unstable because ice will grow at the expense of liquid water by the Wegener–Bergeron–Findeisen

(WBF) mechanism (Morrison et al. 2012), MPCs can be very persistent and often last for several days. The solar radiation field in a cloudy atmosphere is strongly influenced by scattering and absorption by cloud particles as well as by the albedo of the underlying surface (Kahnert et al. 2008). Clouds have a particularly strong nonlinear influence on the surface energy budget in the Arctic (Tsay et al. 1989; Curry and Ebert 1992; Intrieri et al. 2002; Schweiger and Key 1994; Walsh and Chapman 1998; Sandvik et al. 2007), including the timing of the onset of snowmelt (Zhang et al. 1997). The relatively thin boundary layer clouds that are prolific from spring through fall in the Arctic (Lawson et al. 2001; Intrieri et al. 2002; Zuidema et al. 2004; Lawson and Zuidema 2009) transmit (shortwave) sunlight and absorb (long-wave) thermal radiation. The greenhouse effect produced by the thin cloud cover accelerates melting and increases the amount of open water, which absorbs more incoming sunlight than do ice surfaces, setting up a positive feedback

Corresponding author address: Monika Sikand, Department of Physics, Stevens Institute of Technology, 1 Castle Point on Hudson, Hoboken, NJ 07030.
E-mail: msikand@stevens.edu

process that leads to more melting and warming near the surface (Perovich et al. 2008). Clouds have also been observed to play a major role in sea ice loss (Kay and Gettelman 2009), but identifying the reason is a challenge because the sea ice decline over the last 30 yr can be attributed to an energy surplus of just 1 W m^{-2} (Kwok and Untersteiner 2011). Hence, reliable knowledge of cloud microphysical and radiative properties is crucial to understand radiative transfer and the earth's energy budget (Ramanathan et al. 1989).

Previous field campaigns such as the 1998 National Science Foundation (NSF) Surface Heat Budget of the Arctic Ocean (SHEBA) project, National Aeronautics and Space Administration's (NASA's) First International Satellite Cloud Climatology Project (ISCCP) Regional Experiment-Arctic Cloud Experiment (FIRE-ACE), and the Mixed-Phase Arctic Cloud Experiment (M-PACE) provided aircraft measurements using cloud particle imager (CPI) data of MPCs in the Arctic (Lawson et al. 2001; Verlinde et al. 2007). A tethered-balloon system (TBS) was developed and deployed to study MPCs in Ny-Ålesund, Svalbard, Norway, at 78.9°N , 11.9°E in May/June 2008 with support from the atmospheric division of the NSF and the Norwegian Research Council through its International Polar Year (IPY) program and the project IPY– The Observing System Research and Predictability Experiment (THORPEX). The TBS instrument package provided measurements from the basic meteorological sensors as well as miniaturized microphysical and radiation sensors (Stamnes and Storvold 1999). The meteorological sensors measured pressure, temperature, humidity, wind speed, and wind direction. The Norwegian Institute for Air Research's [Norsk Institutt for Luftforskning's (NILU)] lightweight moderate bandwidth filter instrument, named NILU CUBE 4π , was used to measure irradiances in situ at 500 and 800 nm simultaneously on the six sides of a cube. These measurements can be used to estimate the mean intensity (MI). Microphysical cloud data were obtained using a miniaturized version of an airborne CPI. The ability of the CPI to identify the ice particles and cloud droplets during vertical profiling can be used in conjunction with a radiative transfer model (RTM) to improve microphysical retrievals. The Ny-Ålesund deployment demonstrated the utility of the TBS as an observing system capable of making long-term and cost-effective measurements of the microphysical and radiative properties of clouds in the Arctic, and providing vertical profiles of a cloud from the balloon's maximum height all the way down to the surface.

Substantial uncertainties exist in observing these MPCs from the ground and from satellites. These uncertainties are partly due to the heterogeneity of the

underlying surface and partly due to the fact that satellite retrievals of the cloud and surface characteristics are hampered by the complex vertical structure of the atmosphere, including temperature inversions, humidity inversions, and low visible, thermal, and microwave contrast between the clouds and the underlying surface (Curry et al. 2000). To understand the cloud microphysics and the radiative transfer in MPCs, unique observational and modeling studies are required that will help to bridge gaps in the understanding of MPC microphysics, cloud dynamics, and cloud evolution. The temporal behavior of MPCs indicates the changing cloud characteristics related to cloud phase, location, and optical properties. The in situ radiometric and microphysical measurements collected via a TBS can aid in reducing these uncertainties. The uniqueness of the TBS lies in its ability to provide information about MPC characteristics through vertical profiling. This information is also useful in evaluating climate model parameterizations of cloud and radiation processes.

In a previous study (Sikand et al. 2010), we developed a method to estimate the optical properties of MPCs in the Arctic using a forward RTM combined with a manual (trial and error) inversion—an approach that was very labor intensive and time consuming. To alleviate that problem, we have, in this study, extended and automated this methodology to allow for faster retrievals of a more complex cloud scenario, in which the MPC is allowed to evolve with time. This new approach relies on the use of an RTM similar to that used in the previous study (Sikand et al. 2010), but in combination with a standard nonlinear, least squares inverse method as described below. It also allows for a more systematic and accurate analysis of the microphysical and radiometric data collected on the balloon platform by providing an optimal solution.

In this paper we employ this forward-inverse methodology to examine the unique vertical profiles and cloud phase partitioning of a boundary layer MPC system observed on 16 May 2008. Cloud liquid droplets and ice particles have different sizes, shapes, refractive indices, densities, and concentrations (Sun and Shine 1994). The horizontal and the vertical scales over which the two phases exist impact cloud properties and therefore play an important role in determining the climate evolution in the Arctic. In section 2, we discuss and compare the radiometric measurements of two MPC cases: 16 May 2008 analyzed in this study and 29 May 2008 analyzed in the previous study (Sikand et al. 2010). The instruments used to measure the radiometric data were described by Sikand et al. (2010) and Lawson et al. (2011). In section 3, we discuss the RTM constructed to analyze the data obtained on 16 May 2008. Inputs to this RTM were

selected to be consistent with the CPI data. In section 4, we present our methodology and results. In section 5, we discuss the results obtained in this data analysis and model simulation study. Finally, in section 6, we provide a summary along with an outlook on the future use of the TBS in atmospheric studies of microphysical and radiative properties of MPCs.

2. Tethered-balloon radiometric measurements

In Sikand et al. (2010), we attempted to understand the optical properties of the MPCs by analyzing the radiometric measurements from the Ny-Ålesund campaign with the help of a state-of-the-art RTM (Stamnes et al. 1988). The radiometric data can be accessed online (at <http://cdp.ucar.edu/browse/browse.htm?uri=http%3a%2f%2fdataportal.ucar.edu%2fmetadata%2fsit%2fsit.thredds.xml>). The radiometric analysis was used to estimate the optical depth due to ice crystals and water droplets. In this paper, the radiometric TBS measurements obtained for a cloudy situation on 16 May 2008 were analyzed and compared with those obtained on 29 May 2008, reported previously in Sikand et al. (2010). The in situ measurements consisted of 4π irradiances that were used to estimate the mean intensity at 500 and 800 nm, and CPI images that were used to determine the cloud phase. The total downward (TD) irradiance was measured by a collocated, ground-based reference instrument (TriOS RAMSES-ACC-UV Hyperspectral UV/VIS irradiance sensor). The total downward irradiance at the ground was found to be insensitive to the vertical distribution of the cloud particles as long as the total optical depth remained unchanged. However, the mean intensity estimated from the 4π irradiances measured on the TBS was found to be quite sensitive to the vertical cloud particle distribution, and was used to determine the vertical structure of the boundary layer MPC system (Sikand et al. 2010).

Figure 1 shows two very different vertical profiles of boundary layer MPCs. On 29 May 2008 the balloon flew from 1045:02 to 1525:06 UTC in total and reached a maximum altitude of approximately 1177 m at 1352:38 UTC. The solar zenith angle on 29 May 2008 changed from 57.3° at the start of the flight when the balloon was at the ground to 60.2° at the top (approximately 1177 m) and then to 63.8° at the end of the flight when the balloon reached back to the ground. The CPI data obtained during this flight on 29 May 2008 showed a layer of water droplets over ice. During ascent, a general increase in the mean intensity was observed, whereas a reduction in the mean intensity was observed during descent. This behavior in the mean intensity could be due to variations during the time of flight of the solar zenith angle and also

of cloud characteristics, such as cloud-base and cloud-top height, as well as cloud phase and cloud optical depth. The difference between the measured mean intensities at 500 and 800 nm was mainly due to the difference in absorption and scattering properties at the two wavelengths. A drop in the mean intensity with the corresponding decrease in balloon height around 700 m during the ascent could also be due to changing cloud characteristics on this day. The thick lumps in Fig. 1 are due to the balloon floating at a particular location for some time and hence collecting data at that location every 2 s. Two separate profiles between 600 and 750 m in Fig. 1a are due to the balloon going up and down within clouds at this location. However, on 16 May 2008 we observed a very different vertical profile showing no regular trend of mean intensity from the ground all the way up to the maximum altitude of approximately 1350 m. The CPI data obtained during the flight on 16 May 2008 indicated an inhomogeneous distribution of both ice and water droplets. On this day the balloon flew from 0800:38 to 0947:07 UTC in total. The solar zenith angle changed from 63.5° at the start of balloon flight on the ground to 60.5° as the balloon descended to the ground. The slight decrease in the mean intensity with height near the surface could be due to a decrease in the surface albedo “perceived” by the radiometer as the balloon ascended. The balloon stayed for about 20 min near the maximum altitude when the solar zenith angle was close to 61.7° . The change in mean intensity near the maximum altitude could be due to an increase in the concentration of cloud particles at that location (Madronich 1987; de Arellano et al. 1994) caused by a change in cloud phase or proximity to the cloud top (Hobbs and Rangno 1998). The changing pattern of the mean intensity seen in Fig. 1 during the descent could be due to changing cloud optical properties and cloud location. The reduction in the mean intensity around 1000 m during ascent as well as descent combined with CPI data indicates the presence of a significant amount of ice particles in that region. The vertical profiles observed on 16 and 29 May 2008 were obtained during different times of flight, that is, different solar zenith angles. As explained below, the simple model with two cloud layers in fixed positions used to analyze the data obtained on 29 May had to be replaced by a model in which the positions of the cloud layers were allowed to vary in order to get a good match between measured and computed mean intensities on 16 May. Also, the straightforward trial-and-error retrieval scheme employed by Sikand et al. (2010) had to be replaced by a more systematic approach based on nonlinear optimal estimation in order to make sense of the vertical profiles measured on 16 May.

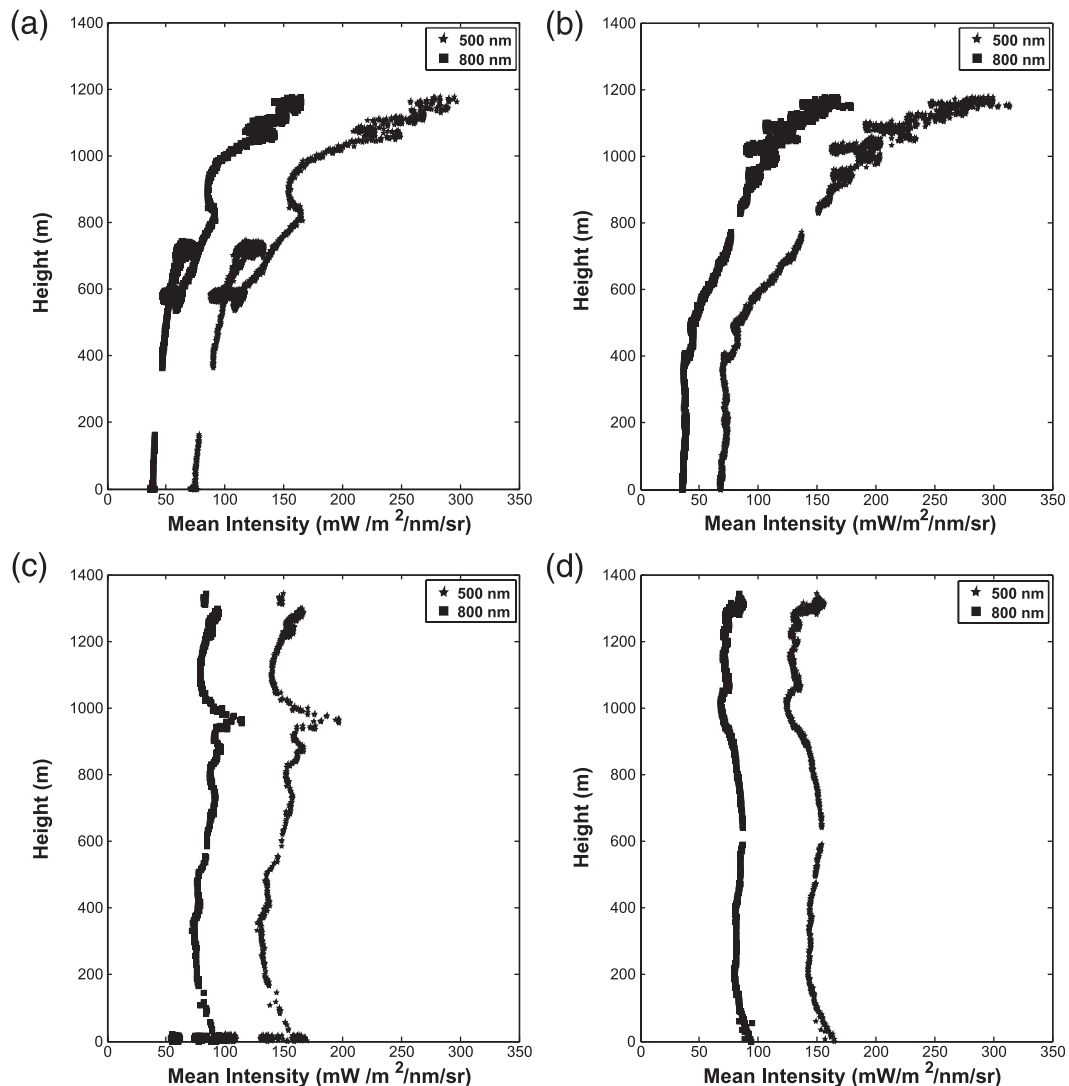


FIG. 1. Estimated mean intensity at 800 (left trace) and 500 nm (right trace) for cloudy-sky conditions during (a),(c) ascent and (b),(d) descent on (a),(b) 29 and (c),(d) 16 May 2008. The vertical profiles observed on 29 and 16 May 2008 were obtained during different times of the day, i.e., different solar zenith angles. The thickness of the curves represents variability in mean intensity with time when the balloon was located at the same altitude.

3. Model simulations

a. Radiative transfer model

A plane-parallel inhomogeneous (multilayer) RTM was used to simulate the radiation transport in the atmosphere in a manner that could be compared to the observations. To simulate the TBS and ground-based radiometric measurements, the cloud was represented by vertically stratified layers of liquid droplets and ice particles, so that one could compute irradiances and mean intensities by using an azimuthally averaged version of the radiative transfer equation, which describes the transfer of the diffuse monochromatic solar intensity I in a scattering and absorbing plane-parallel atmosphere. To incorporate

clouds in a plane-parallel RTM, one may use multiple stratified layers. If one adopts a sufficiently large number of layers, then this approach, which has been used in a number of studies (e.g., Tsay et al. 1989, 1990), can account for significant vertical variations in gaseous absorption and scattering as well as in the size distribution of water droplets and in the size and shape distributions of ice particles and their associated radiative effects. Based on these considerations, we constructed a RTM that included radiative interactions with atmospheric gases [see section 3b(1)] as well as parameterized treatments of scattering and absorption by cloud particles [see section 3b(2)].

To solve the radiative transfer equation, we employed the radiative transfer code Discrete Ordinate Radiative

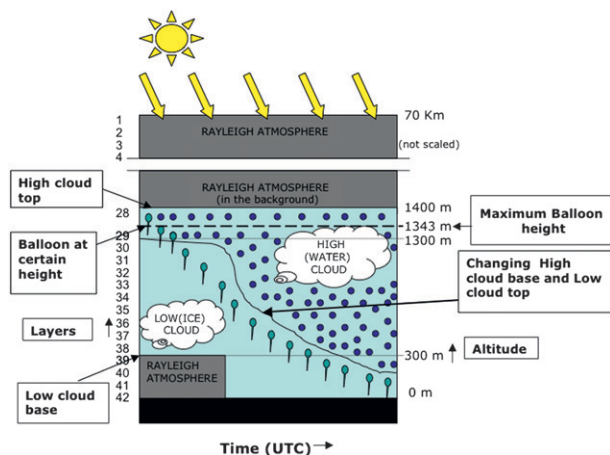


FIG. 2. Schematic illustration of a two-layer cloud model, consisting of a low ice cloud (LC) and high liquid water cloud (HC), embedded in a background clear-sky (molecular) atmosphere, used to analyze the TBS data observed on 16 May 2008. Based on the CPI images, the LC base was determined to be at about 300 m and the HC base at about 1300 m. The HC base and LC top boundary were allowed to change with time (UTC) and brought closer to ground to achieve agreement between simulated and measured mean intensities.

Transfer (DISORT) (Stamnes et al. 1988), which was well suited for our purpose. The input to the model included solar irradiance data obtained from NASA’s Solar Radiation and Climate Experiment (SORCE) was taken to be approximately $1900 \text{ mW m}^{-2} \text{ nm}^{-1}$ at 500 nm and $1100 \text{ mW m}^{-2} \text{ nm}^{-1}$ at 800 nm. Other input parameters included the cosine of the solar zenith angle calculated from the National Oceanic and Atmospheric Administration’s (NOAA’s) solar position calculator (at <http://www.srrb.noaa.gov/highlights/sunrise/azel.html>) and a Lambertian surface albedo, which was estimated from measurements taken under clear-sky conditions (Sikand 2012).

b. Inherent optical properties (IOPs)

1) CLEAR (CLOUD FREE) BACKGROUND ATMOSPHERE IOPS

We used a stratified atmosphere of 42 layers as a background. The atmospheric transmittance model Moderate Resolution Atmospheric Transmission (MODTRAN), a computer program designed to simulate atmospheric propagation of electromagnetic radiation in the $100\text{--}50\,000 \text{ cm}^{-1}$ ($0.2\text{--}100 \mu\text{m}$) spectral range, was used to estimate the radiative interactions with gases. Our atmospheric model represented the vertical variations of the atmosphere with a height resolution of 100 m from the ground up to 2000 m and a coarser height resolution from 2 up to 70 km (see Fig. 2). The MODTRAN transmittance model was used to compute the scattering

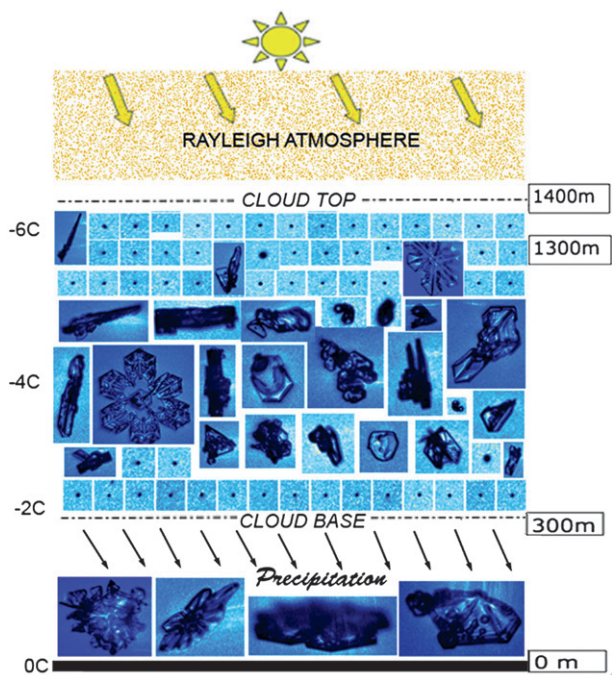


FIG. 3. The vertical profile of MPC particle images consisting of ice crystals and liquid droplets observed during the descent on 16 May 2008.

optical depth τ_{scatter} and the total optical depth τ_{total} at 500 and 800 nm for molecular (Rayleigh) scattering and absorption in each of the 42 atmospheric layers.

To simulate the radiation field at the location of the 4π radiometer deployed on the TBS platform, the appropriate altitude to be used in the model was calculated from the pressure data collected by the meteorological package.

2) CLOUD IOPS

Figure 2 shows a schematic illustration of the atmospheric model with cloud layers embedded within the 42 layers of clear atmosphere. The cloud model was based on images observed by the CPI, which showed vertical profiles of MPCs consisting of ice crystals with a variety of sizes, shapes, and degree of riming as well as liquid water droplets. The amount of ice in the MPCs varied considerably with altitude, but it did not appear to be a function of temperature. On 16 May 2008 the balloon flight started at 0800:38 UTC at a solar zenith angle of 63.5° . The balloon moved continually up and reached a maximum altitude of approximately 1343 m at 0857:45 UTC and then stayed around 1300 m for approximately 20 min. At the top of the flight, the solar zenith angle was close to 61.7° . As the balloon descended from the 1300 m level at 0903 UTC, the CPI images revealed a predominance of liquid water droplets down to temperatures of -6.4°C (see Fig. 3).

Liquid-water-topped clouds are likely to be common in the Arctic, and they may play an important role in the radiation balance of the region (Hobbs and Rangno 1998). As the balloon descended farther, the CPI images began to show presence of mostly ice particles below 1300 m, and that trend continued down to approximately 300 m, where the temperature was about -2°C (see Fig. 3). As indicated in Fig. 3, a few water droplets appear again around 300 m, and this pattern persists all the way to near the surface. Based on the CPI data obtained during the descent on 16 May 2008 (see Fig. 3), we constructed a two-layer cloud model. As shown in Fig. 2, in this two-layer cloud model, we assumed that the lower layer consisted primarily of ice particles and stretched from 300 to 1300 m. We further assumed that the upper layer consisted primarily of water droplets and stretched from 1300 to 1400 m. Since there were a few water droplets in the lower layer, which is assumed to consist primarily of ice, and a few ice crystals in the upper layer, which is assumed to consist primarily of liquid water, the results presented below will have some uncertainties related to the validity of the assumption that the upper layer consisted of liquid particles only and the lower layer of ice particles only. The two layers had slightly different optical properties. The first moment of the scattering phase function, the so-called asymmetry factor g , is often adopted to describe the angular scattering or phase function of cloud particles. The asymmetry factor and the single-scattering albedo were parameterized on the basis of Mie theory for liquid water clouds in terms of the effective droplet size (Hu and Stamnes 1993). For computations of integrated radiative quantities, such as irradiances and mean intensities, used in the data analysis in this paper, the details of the phase function are not important, and the first moment of the phase function—that is, the asymmetry factor—is sufficient to provide adequate results. We may therefore use the simple Henyey–Greenstein phase function, which depends only on the asymmetry factor, to characterize the angular distribution of the scattered radiation. Since the asymmetry factor for ice particles is typically smaller than for liquid droplets (Sun and Shine 1994; Fu 1996; Curry et al. 2000; Garrett et al. 2001; Kahnert et al. 2008), we let the asymmetry factor for the cloud particles in the ice cloud layer be smaller ($g = 0.75$; Garrett et al. 2001) than in the liquid water cloud layer ($g = 0.80$). The single-scattering albedo at both 500 and 800 nm was assumed to be 0.999. Since the optical depth decreases when a liquid cloud layer transforms into the solid phase (Curry and Ebert 1992), the lower ice cloud layer may typically be expected to be optically thinner than the higher liquid water layer even though its vertical extent was assumed to be small. Based on 4π measurements

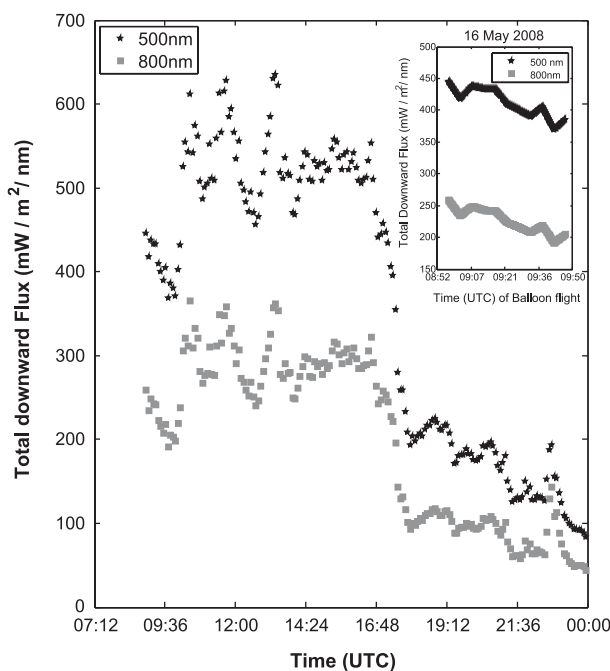


FIG. 4. Total downward irradiance measured on 16 May 2008 with a ground-based spectrometer (RAMSES) at 500 (black stars) and 800 nm (gray squares). In the inset the total downward flux interpolated at 500 (black stars) and 800 nm (gray squares) is shown with time to match the balloon flight time.

during a balloon flight on 4 May 2008 under clear-sky conditions, the surface albedo was estimated to be 0.75 at 500 nm and 0.7 at 800 nm (Sikand 2012).

4. Methodology and results

The total downward irradiance measured by the ground-based radiometer was found to be insensitive to the vertical distribution of the cloud particles (liquid or ice). We first used the ground radiometer measurement shown in Fig. 4 to estimate the total optical depth of the cloud system. The ground instrument provided the total downward irradiance every 5 min, whereas the balloon radiometer provided mean intensity data every 2 s. Because of inconsistency in the timing of the data collection on the balloon and on the ground, we interpolated the measured total downward irradiance to the balloon flight time (see inset of Fig. 5). In Sikand et al. (2010), the cloud model consisted of two cloud layers with fixed positions in the background of 42 atmospheric layers used to describe the clear-sky atmosphere. In the cloud model used in this paper, the positions of the two cloud layers were allowed to evolve with time. We also found through RTM simulations, that the total downward irradiance reaching the surface did not depend on the cloud location, and that it remained the same irrespective of the vertical positions

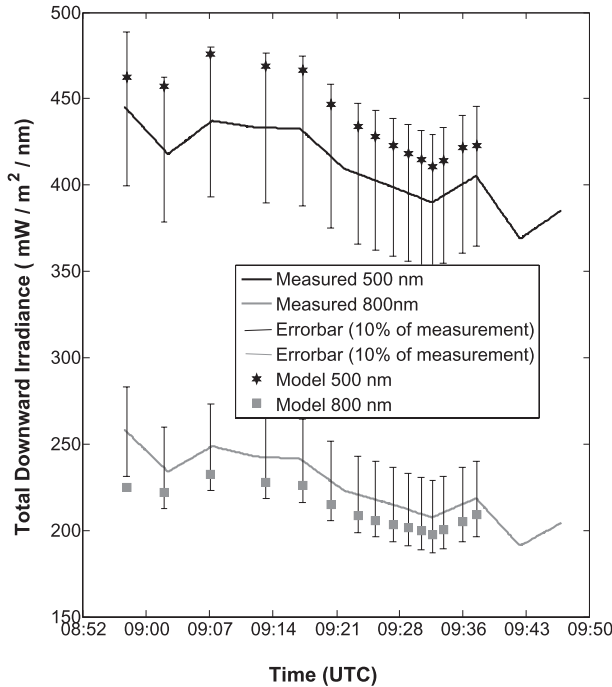


FIG. 5. The total downward irradiances computed from the two-layer cloud RTM agree within 10% with the interpolated measured total downward irradiances during the balloon flight (time in UTC). The total downward irradiance measured by the ground-based radiometer was found to be insensitive to the vertical distribution of the cloud particles (liquid or ice). The model results at 500 (black stars) and 800 nm (gray squares) were inferred using a nonlinear least squares solution approach as discussed in the text.

of the two cloud layers as long as the total optical depth of the MPC was the same. However, the mean intensity at a particular height varied because of changes in the positions of the two cloud layers. In Sikand et al. (2010), the optical depths of the two cloud layers, which were in fixed positions, were varied until the best match was obtained between measured and simulated mean intensities. Attempting to obtain a match between measured and simulated mean intensities for the data collected on 16 May 2008 proved to be impossible with the two cloud layers in fixed positions. Therefore, in this paper, we extended this methodology to allow the positions of the two cloud layers to vary as the cloud system evolved with time.

The manual (trial and error) approach used to analyze the data obtained on 29 May 2008 with fixed cloud positions, as described in Sikand et al. (2010), was found to be inadequate to analyze the data obtained on 16 May 2008. The forward-inverse modeling approach used in the analysis in this paper allows for adjustment of the positions of the cloud layers as needed to obtain a good fit of the measured mean intensities to the simulated ones. To estimate the cloud optical depth in the two cloud

layers from the complex vertical profile of the mean intensities obtained on 16 May 2008, we used a nonlinear least squares solution approach. The irradiance and the mean intensity were computed by using a forward RTM based on DISORT (Stamnes et al. 1988) with IOPs specified as described above. Although the radiative transfer equation is linear, the response of the computed radiative quantities depends nonlinearly on the retrieval parameters, such as the cloud optical depth.

An approximate solution to the retrieval problem can be obtained by linearizing the forward model $\mathbf{F}(\mathbf{x})$ about some reference state \mathbf{x}_0 using a first-order Taylor series expansion (Rodgers 2000) as shown:

$$\mathbf{y} = \mathbf{F}(\mathbf{x}); \tag{1}$$

and

$$\mathbf{F}(\mathbf{x}) - \mathbf{F}(\mathbf{x}_0) \approx \mathbf{J}(\mathbf{x} - \mathbf{x}_0); \quad \mathbf{J} = \frac{\partial \mathbf{F}(\mathbf{x})}{\partial \mathbf{x}}. \tag{2}$$

Here, the data vector \mathbf{y} consisted of four simultaneous observations composed the mean intensities at 500 and 800 nm (two measurements) estimated from the 4π radiometer deployed on the balloon, and the irradiances at 500 and 800 nm (two measurements) measured by the ground-based spectrometer. The state vector \mathbf{x} consisted of the optical depths of the two cloud layers, and \mathbf{J} was the Jacobian matrix consisting of irradiance or mean intensity variations (partial derivatives) with respect to the state vector. The cloud optical depths on 16 May 2008 were then estimated by a set of linear algebraic equations, that is,

$$\mathbf{y} = \mathbf{F}(\mathbf{x}) \approx \mathbf{J}\mathbf{x}. \tag{3}$$

The least squares solution of Eq. (3) can be obtained from the following set of normal equations

$$\mathbf{x} = (\mathbf{J}^T \mathbf{J})^{-1} \mathbf{J}^T \mathbf{y}. \tag{4}$$

Since the problem is nonlinear, we solve it by iteration as shown:

$$\mathbf{x}_{i+1} = \mathbf{x}_i + (\mathbf{J}_i^T \mathbf{J}_i)^{-1} \mathbf{J}_i^T [\mathbf{y} - \mathbf{F}(\mathbf{x}_i)], \tag{5}$$

where the number of iterations are determined by the need to minimize the cost function $\Phi(\mathbf{x})$, which is the difference between the measurements and the forward model, as shown:

$$\Phi(\mathbf{x}) = [\mathbf{y} - \mathbf{F}(\mathbf{x})]^T \mathbf{S}_\epsilon^{-1} [\mathbf{y} - \mathbf{F}(\mathbf{x})] \tag{6}$$

or

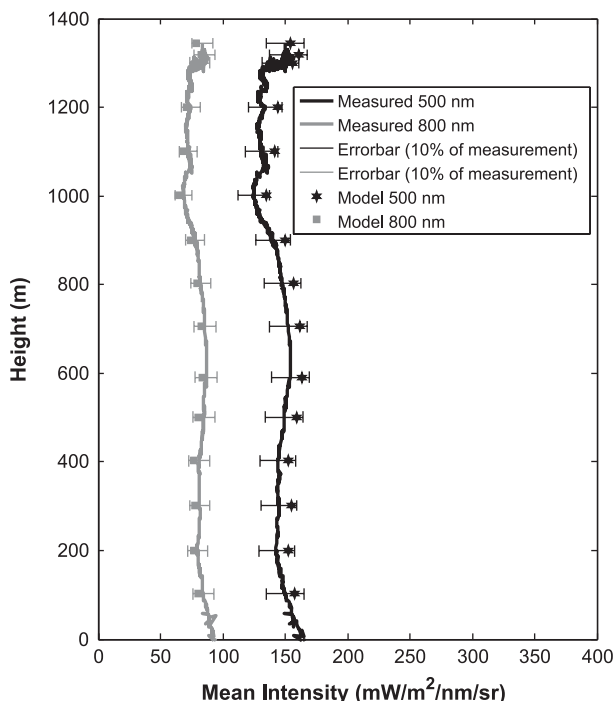


FIG. 6. Measured mean intensity profiles of an MPC system observed on 16 May 2008 at 500 (black) and 800 nm (gray). Modeled mean intensities (stars: 500 nm, squares: 800 nm) agree within 10% with the measurements. The optical depths and positions of two cloud layers were varied in this forward-inverse modeling approach until the best match was obtained between measured and simulated mean intensities.

$$\Phi(\mathbf{x}) = [\mathbf{y} - \mathbf{F}(\mathbf{x})]^T [\mathbf{y} - \mathbf{F}(\mathbf{x})] \quad (7)$$

if we set the measurement error covariance matrix to $\mathbf{S}_\epsilon \equiv \mathbf{I}$. The optical depths of the two cloud layers at 500 and 800 nm were estimated using this forward-inverse modeling approach, which provided the best simultaneous match to the balloon measurements of the mean intensities at a particular time (height) and the total downward irradiances measured with the upward-looking radiometer on the ground.

At the maximum altitude where the balloon spent a considerable amount of time, we were able to get a good match between the computed and measured 4π mean intensities with fixed cloud boundaries. As the balloon began to descend, Fig. 6 shows a reduction in the mean intensity just below the maximum altitude. However, as the balloon descended farther, it became challenging to achieve good agreement between computed and measured 4π mean intensities. This difficulty could be due to changing optical properties of the clouds, cloud movement, assumptions of surface albedo on a cloudy day based on clear-sky results, asymmetry factor values, or

other/unknown factors. During the descent, we observed liquid droplets in CPI images between 0903 and 0904 UTC when the balloon was located near 1300 m. As the balloon reached altitudes below 1300 m, the CPI images showed a predominance of ice particles. Hence, a two-layer cloud model consisting of a low ice cloud with a cloud base around 300 m and a high liquid water cloud with a cloud base around 1300 m was constructed. As time progressed during the descent, we observed a thin layer of the liquid droplets at 0934 UTC near 300 m (cloud base). Since the cloud appeared vertically inhomogeneous, we allowed the boundaries of the two cloud layers to move toward the surface with time in order to achieve agreement between the simulated and measured mean intensities. We assumed that ice from the cloud base at 300 m extended to the surface as the balloon descended with time and as indicated schematically in Fig. 2. This adjustment of the lower cloud layer closer to the ground as time progressed during TBS descent was based on the assumption that the cloud drops observed at the cloud base precipitates as ice through the cloud base all the way to the surface (Lawson et al. 2001; Curry et al. 1996). We found that as the balloon descended farther, a good match between measured and simulated mean intensities could be obtained by (i) increasing the vertical extent of the higher liquid water cloud toward the surface, (ii) reducing the vertical extent of the lower ice cloud toward the surface, and (iii) constraining the top of the lower cloud to be located just above the balloon height to provide better control on the tuning of the two cloud optical depths.

By allowing the cloud boundaries to adjust in this manner, we were able to obtain a good match between the mean intensities inferred from the balloon 4π radiometer data and the total downward irradiance measured on the ground by the upward-looking radiometer. The total optical thickness of the two cloud layers retrieved in this manner during the balloon descent are shown in Fig. 7. The partitioning of the optical depths of the two cloud layers is also shown in Fig. 7 as a function of time during balloon descent. The maximum cloud optical depth estimated from a good match between measured and simulated radiometric data was found to be approximately 32 at 500 nm and 31 at 800 nm on 29 May 2008 (Sikand et al. 2010). By contrast, on 16 May 2008 it was found to be approximately 18 at 500 nm as shown in Fig. 7 and approximately 17 at 800 nm.

5. Discussion and sensitivity analysis

The vertical profile of the mean intensity observed on 16 May 2008 (Fig. 1) shows that it increased and decreased irregularly with altitude during the balloon flight.

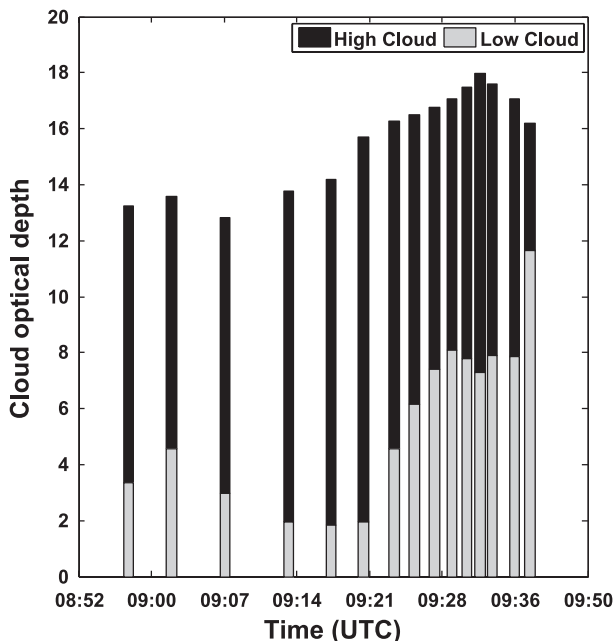


FIG. 7. Partitioning of LC (gray) and HC (black) optical thicknesses. The cloud optical thickness at 500 nm was estimated using a nonlinear least squares solution approach.

This behavior is due to changing cloud characteristics including optical properties as well as cloud-top and cloud-base heights. The tethered balloon spent about 20 min at the maximum altitude around 1300 m during this flight where the CPI showed a predominance of water droplets. This feature is consistent with the analyses of aircraft data by Hobbs and Rangno (1998), who showed that many MPCs in the Arctic attain a steady-state consisting of a liquid-topped cloud that continually precipitates ice. Such a structure appears to be common, as shown by the SHEBA lidar data (Intrieri et al. 1999) and by the Department of Energy Atmospheric Radiation Measurement Program (DOE ARM) North Slope of Alaska (NSA) radar and lidar data. We also observed an increase in the mean intensity near the ground that could be due to an increase in the surface albedo perceived by the radiometer as the balloon descended. Uncertainties in the results could be due to changing optical properties of the clouds, cloud movement, assumptions regarding surface albedo on a cloudy day based on clear-sky results, adopted asymmetry factors, and other/unknown factors. Simulations indicate that the retrieved low cloud optical depth changes by about 15%–20% and the retrieved high cloud optical depth by about 20%–30% when the surface albedo or asymmetry factor changes by 10%.

By adjusting the boundaries and the optical depths of the two cloud layers in the RTM, we achieved a good

match between mean intensities simulated by the RTM and inferred from the 4π radiometer measurements. We used this approach to estimate the optical thickness of the two cloud layers, employing the nonlinear least squares fitting procedure described in section 4. The total optical thickness estimated from the 4π radiometer measurements was constrained to be the same as that measured by the upward-looking radiometer on the ground. This procedure provided the optical thickness of the cloud layers at a particular instant in time. To obtain a good match, it was necessary to allow the location of the base of the lower cloud to move closer to the ground, which led to an increase in its retrieved optical depth as shown in Fig. 7. In this manner the 4π radiometer data collected by the NILU CUBE instrument were used to estimate the partitioning of the optical depth between liquid water and ice in the Arctic MPC. By vertical profiling the 4π radiometer data also helped us estimate the vertical extent of the cloud layers as a function of time as indicated in Fig. 2. Such information is very challenging to retrieve from satellites or aircraft.

To understand the response of our model to perturbations in optical parameters, we evaluated the sensitivity of the computed downward irradiance at the surface as well as the mean intensity at the location of the TBS platform due to changes in individual cloud layer optical thicknesses when the total optical thickness was constrained to be constant. We perturbed the optical thickness of the low cloud as well as the high cloud in steps of 0.1 until we reached two extremes as follows. First, we increased the optical thickness of the low cloud in steps of 0.1 but constrained it to be slightly less than that of the high cloud, and then we decreased it in steps of 0.1 until it became very thin. By constraining the low cloud optical depth to be less than that of the high cloud, we maintained consistency in our two-layer cloud model based on CPI images. Figure 8 shows the estimated sensitivity of the total downward irradiance as well as the mean intensity due to the perturbation in cloud optical thickness at 500 and 800 nm. We found that the total downward irradiance reaching the surface was not very sensitive (within 4%) to changes in individual cloud layer optical thicknesses of the cloud system as long as the total cloud optical thickness remained the same. However, the mean intensity at different times (balloon heights) showed a sensitivity of about 25%. Thus, the mean intensity data collected with the 4π instrument on the TBS were quite sensitive to the partitioning of the optical thicknesses between the two cloud layers. This kind of information could be useful in future TBS campaigns to infer the total cloud optical depth and its partitioning between liquid water and ice.

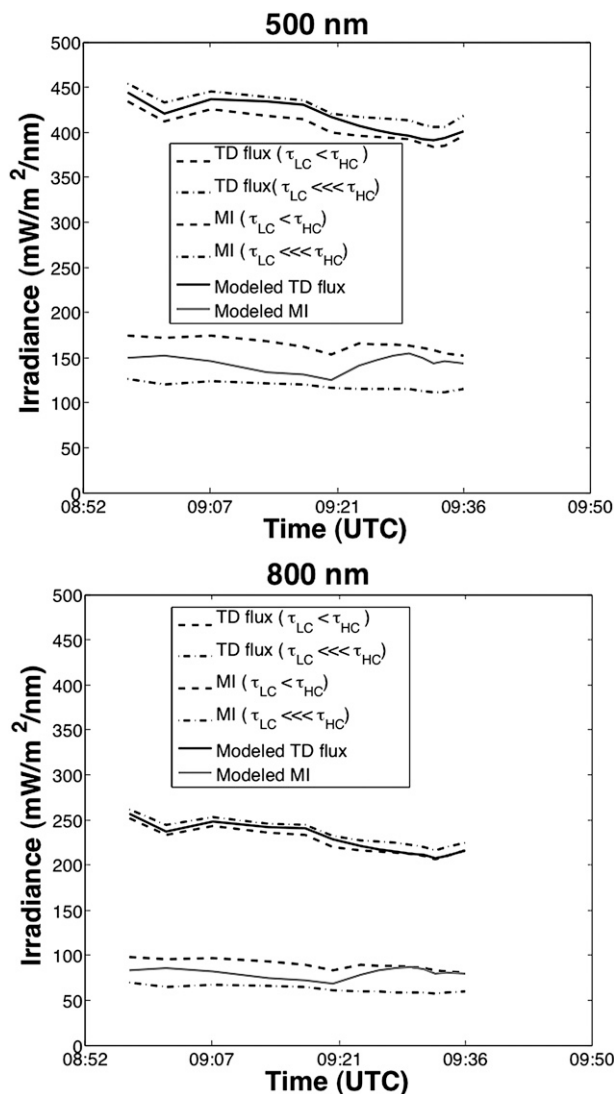


FIG. 8. Estimated sensitivity (due to perturbations in optical depths in the two cloud layers) of the total downward (TD) irradiance (solid black) and mean intensity (MI) (solid gray) at 500 and 800 nm. The total optical thickness is constrained to be the same as before the perturbations. The TD is not very sensitive to a change in optical depth of the two cloud layers and varies within 4%. The MI, in contrast, has been found to be quite sensitive to a change in optical depth of the two cloud layers and varies within 25%. The area around the solid line is unsymmetric due to the changing positions of the cloud layers as well as the changing location of the NILU-CUBE instrument, whose response is being simulated with time.

6. Summary and outlook

a. Summary

A novel TBS (Sikand et al. 2010; Lawson et al. 2011), capable of measuring true vertical profiles and time series of microphysical and radiometric properties, was used to collect data in May–June 2008 at Ny-Ålesund,

Norway (78.9°N, 11.9°E). The powered-tether approach allows for long time series and uninterrupted operation. This feature is especially valuable in cold climates where battery lifetime is limited. Such in situ measurements are not feasible using aircraft or ground-based remote sensing instruments only. The radiometric data collected via two instruments—namely, the NILU-CUBE 4π radiometer on the TBS and the RAMSES radiometer on the ground—were analyzed to retrieve optical properties of MPCs observed on 16 May 2008 using an RTM. The CPI data were used to construct an RTM that included scattering and absorption by cloud particles embedded in a background clear-sky (molecular) atmosphere. The RTM was used in conjunction with the ground-based irradiance measurements to estimate the total optical thickness of the cloud system as a function of time, irrespective of the vertical distribution of ice particles and liquid droplets. The mean intensity measured on the TBS was used in conjunction with the RTM to estimate the time evolution of the vertical distribution of ice particles and liquid droplets.

Our analysis of the CPI and radiometer data for the flight on 16 May 2008 can be summarized as follows:

- an increase in the vertical extent of the upper cloud layer and a reduction in the vertical extent of the lower cloud layer was needed in order to obtain a good match between measured and simulated mean intensities;
- the optical thickness of the upper liquid cloud gradually became smaller toward the end of the balloon flight;
- the maximum total cloud optical depth on 16 May 2008 was found to be approximately 18 at 500 nm as shown in Fig. 7 and approximately 17 at 800 nm.

It should be noted that in our analysis, we used a two-layer cloud model with liquid water only in the upper layer and ice particles only in the lower layer. Since the CPI data indicated that there were a few water droplets in the lower layer, assumed to be primarily ice, and a few ice crystals in the upper layer, assumed to be primarily liquid water, the results presented in this paper will have some uncertainties related to the validity of these assumptions.

b. Outlook

The TBS platform can be used to deploy a variety of instrument packages into the atmospheric boundary layer. Here is our “dream list” of potential instruments that could be deployed on the TBS. This list includes, but is not limited to, counters of cloud condensation nuclei (CCN) and ice-forming nuclei (IFN) as well as cameras for monitoring the surface conditions, filters for collecting and analyzing ice nuclei, a particle imaging

probe that extends to centimeter-size particles, and a new miniaturized (<2 kg) in situ cloud lidar currently under development.

The CPI used in the current TBS weighs 7 kg. A miniature CPI, designed to fly on a small, unmanned aerial system, is now under development and weighs less than 2 kg. Adoption of this new CPI technology into the TBS would increase the payload potential by 5 kg and thus enable one to add new instruments, such as those discussed above.

The 4π radiometer deployed in May 2008 at Ny-Ålesund had only two channels. A next-generation radiometer that will include additional near-infrared (NIR) channels is now being contemplated. One idea is to expand the wavelength range into the NIR (potentially up to 1650 nm). While silicon photodiodes are optimum over the wavelength range from 300 to 1000 nm, beyond 1050 nm different detectors, such as indium gallium arsenide (InGaAs) photodiodes, with bandwidths larger than 20 nm may be required. NIR measurements typically necessitate detectors with thermoelectric or cryogenic cooling. The use of uncooled detectors, which have a high dark current but also a high spectral response, could be a possibility. Also, efforts should be made to reduce the weight of the instrument by using lightweight material for the mechanical frame, and the feasibility of redesigning the instrument to make it more compact should be explored. Other desirable improvements include the addition of a GPS/three-axis compass to record the orientation of the sensor heads as well as accurate temperature sensors to allow for corrections of temperature effects.

The present winch, built for the 1998 SHEBA project, was dimensioned for a tether designed to carry high currents that would heat the tether for deicing purposes. The high-current approach necessitated a large drum that would provide large surface area exposure for adequate cooling of the tether. It was found that the high current was unnecessary for deicing and a lower-current approach was subsequently adopted. Since the high current and large drum are no longer needed, a smaller drum could be fabricated that would considerably reduce the size and weight of the TBS and allow it to be transported on commercial airliners with limited cargo door access dimensions.

Finally, it would be useful to develop reliable data-processing tools that could be used to turn the data collected by the TBS instruments into meaningful geophysical parameters. For example, flow modeling and calibration techniques need to be developed to better quantify CPI collection efficiency of water and ice particles, which is a complex function of particle type and size, fall velocity, ambient wind speed, and sample tube

angle of attack. Quantified water drop and ice particle size distributions could then be used to compute total water drop and ice particle concentrations, liquid water content (LWC), ice water content (IWC), effective particle sizes, and extinction coefficients, and combined values of these parameters. The asymmetry factor can be derived from Mie scattering theory for the liquid water drop portion of the cloud and from lookup tables that relate CPI particle shape to the scattering phase function for the ice portion of the cloud (Lawson et al. 1998; Shcherbakov et al. 2006). Also, data collected with the 4π radiometer, as discussed in this paper, in conjunction with the CPI data can be used to infer the total optical depth and its partitioning between liquid water and ice. These optical properties (effective particle size, liquid/ice water path, extinction coefficient, optical depth, and asymmetry factor), which can be derived from future TBS measurements, are the inputs required by climate models.

In attempting this difficult experiment, we learned some lessons that would be helpful in future TBS campaigns. One of the significant lessons learned was that making in-cloud measurements using a “new” delivery system brought out issues that one does not need to consider with conventional aircraft platforms. For example, when sampling from the TBS platform, particle trajectories (and thus collection efficiencies) are a function of both particle fall speed and wind velocity. Such considerations are generally absent when flying at aircraft speeds. Another example is snow loading on the top of the balloon, which can cause it to pitch up (or down) and affect the sampling. We considered icing on the balloon, which did not turn out to be a problem, but snow loading did require cleaning snow from the balloon. The bottom line is that, while it may appear to be much simpler to sample from a “stationary” platform, such as a tethered balloon, and perhaps this will be the case once the learning curve is ascended, there is much to be learned in the meantime.

To put future TBS measurements into perspective, we close by noting that (i) MPCs have been found to cover large areas in the Arctic; (ii) MPCs can be very persistent and last for several days; and (iii) a proper treatment of clouds in the Arctic, including MPCs, is a prerequisite for reliable estimates of climate forcing, the onset of snowmelt, the rate of snow/ice ablation, the length of the melt season (Zhang et al. 1996, 1997; Shupe 2011; Morrison et al. 2012), and ultimately the fate of sea ice and ice sheets in a changing climate.

Acknowledgments. This work was supported by the National Science Foundation (NSF) Physical Meteorology Program Grant ATM-0752893 to Stevens Institute

of Technology as well as through NSF Grant DGE-0742462 supporting GK-12 fellowships. The work was also supported by the Norwegian Research Council through its International Polar Year program and the project IPY-THORPEX (Grant 175992/S30, www.ipythorpex.no). The support of the National Science Foundation and the Norwegian Research Council is gratefully acknowledged. We have benefitted from constructive suggestions provided by two anonymous reviewers, which led to significant improvements of the paper.

REFERENCES

- Curry, J. A., and E. E. Ebert, 1992: Annual cycle of radiative fluxes over the Arctic Ocean: Sensitivity to cloud optical properties. *J. Climate*, **5**, 1267–1280.
- , W. B. Rossow, D. Randall, and J. L. Schramm, 1996: Overview of Arctic cloud and radiation characteristics. *J. Climate*, **9**, 1731–1764.
- , J. O. Pinto, T. Benner, and M. Tschudi, 1997: Evolution of the cloudy boundary layer during the autumnal freezing of the Beaufort Sea. *J. Geophys. Res.*, **102** (D12), 13 851–13 860.
- , and Coauthors, 2000: FIRE Arctic Clouds Experiment. *Bull. Amer. Meteor. Soc.*, **81**, 5–29.
- de Arellano, J. V.-G., P. G. Duynkerke, and M. V. Weele, 1994: Tethered-balloon measurements of actinic flux in a cloud-capped marine boundary layer. *J. Geophys. Res.*, **99** (D2), 3699–3705.
- de Boer, G., E. W. Eloranta, and M. D. Shupe, 2009: Arctic mixed-phase stratiform cloud properties from multiple years of surface-based measurements at two high-latitude locations. *J. Atmos. Sci.*, **66**, 2874–2887.
- Fu, Q., 1996: An accurate parameterization of the solar radiative properties of cirrus clouds for the climate models. *J. Climate*, **9**, 2058–2082.
- Garrett, T. J., P. V. Hobbs, and H. Gerber, 2001: Shortwave, single-scattering properties of Arctic ice clouds. *J. Geophys. Res.*, **106** (D14), 15 155–15 172.
- Hobbs, P. V., and A. L. Rangno, 1998: Microstructures of low and middle level clouds over the Beaufort Sea. *Quart. J. Roy. Meteor. Soc.*, **124**, 2035–2071.
- Hu, Y., and K. Stamnes, 1993: An accurate parameterization of the radiative properties of water clouds suitable for use in climate models. *J. Climate*, **6**, 728–742.
- Intrieri, J. M., C. W. Fairall, and B. J. McCarty, 1999: Lidar-derived Arctic cloud properties and radiation measurements during the polar winter season at SHEBA. Preprints, *Fifth Conf. on Polar Meteorology and Oceanography*, Dallas, TX, Amer. Meteor. Soc., 154–157.
- , —, M. D. Shupe, P. O. G. Persson, E. L. Andreas, P. S. Guest, and R. E. Moritz, 2002: An annual cycle of Arctic surface cloud forcing at SHEBA. *J. Geophys. Res.*, **107**, 8039, doi:10.1029/2000JC000439.
- Kahnert, M., A. D. Sandvik, M. Biryulina, J. J. Stamnes, and K. Stamnes, 2008: Impact of ice particle shape on short-wave radiative forcing: A case study for an Arctic ice cloud. *J. Quant. Spectrosc. Radiat. Transfer*, **109**, 1196–1218.
- Kay, J. E., and A. Gettelman, 2009: Cloud influence on and response to seasonal Arctic sea ice loss. *J. Geophys. Res.*, **114**, D18204, doi:10.1029/2009JD011773.
- Kwok, R., and N. Untersteiner, 2011: New high-resolution images of summer sea ice. *Phys. Today*, **64**, 36–41.
- Lawson, R. P., and P. Zuidema, 2009: Aircraft microphysical and surface-based radar observations in summertime Arctic clouds. *J. Atmos. Sci.*, **66**, 3505–3529.
- , A. J. Heymsfield, S. M. Aulenbach, and T. L. Jensen, 1998: Shapes, sizes and light scattering properties of ice crystals in cirrus and a persistent contrail during SUCCESS. *Geophys. Res. Lett.*, **25**, 1331–1334.
- , B. A. Baker, C. G. Schmitt, and T. L. Jensen, 2001: An overview of microphysical properties of Arctic clouds observed in May and July 1998 during FIRE ACE. *J. Geophys. Res.*, **106** (D14), 14 989–15 014.
- , and Coauthors, 2011: Deployment of a tethered-balloon system for microphysics and radiative measurements in mixed-phase clouds at Ny-Ålesund and South Pole. *J. Atmos. Oceanic Technol.*, **28**, 656–670.
- Madronich, S., 1987: Photodissociation in the atmosphere 1. Actinic flux and the effects of ground reflections and clouds. *J. Geophys. Res.*, **92** (D8), 9740–9752.
- Morrison, H., G. de Boer, G. Feingold, J. Harrington, M. D. Shupe, and K. Sulia, 2012: Resilience of persistent Arctic mixed-phase clouds. *Nat. Geosci.*, **5**, 11–17.
- Perovich, D. K., J. A. Richter-Menge, K. F. Jones, and B. Light, 2008: Sunlight, water and ice: Extreme Arctic sea ice melt during the summer of 2007. *Geophys. Res. Lett.*, **35**, L11501, doi:10.1029/2008GL034007.
- Ramanathan, V., B. R. Barkstrom, and E. F. Harrison, 1989: Climate and the earth's radiation budget. *Int. Agrophys.*, **5**, 171–181.
- Rangno, A. L., and P. V. Hobbs, 2001: Ice particles in stratiform clouds in the Arctic and possible mechanisms for the production of high ice concentrations. *J. Geophys. Res.*, **106** (D14), 15 065–15 075.
- Rodgers, C. D., 2000: *Inverse Methods for Atmospheric Sounding: Theory and Practice*. Series on Atmospheric, Oceanic and Planetary Physics, Vol. 2, World Scientific, 240 pp.
- Sandvik, A., M. Biryulina, N. G. Kvamstø, J. J. Stamnes, and K. Stamnes, 2007: Observed and simulated microphysical composition of Arctic clouds: Data properties and model validation. *J. Geophys. Res.*, **112**, D05205, doi:10.1029/2006JD007351.
- Schweiger, A., and J. R. Key, 1994: Arctic Ocean radiative fluxes and cloud forcing estimates from the ISCCP C2 cloud dataset. *J. Appl. Meteor.*, **33**, 948–963.
- Shcherbakov, V., J. F. Gayet, B. Baker, and R. P. Lawson, 2006: Light scattering by single natural ice crystals. *J. Atmos. Sci.*, **63**, 1513–1525.
- Shupe, M. D., 2011: Clouds at Arctic atmospheric observatories. Part II: Thermodynamic phase characteristics. *J. Appl. Meteor. Climatol.*, **50**, 645–661.
- , S. Y. Matrosov, and T. Uttal, 2006: Arctic mixed-phase cloud properties derived from surface-based sensors at SHEBA. *J. Atmos. Sci.*, **63**, 697–711.
- Sikand, M., 2012: Optimal estimation of optical properties of mixed phase Arctic clouds observed from a tethered balloon platform. Ph.D. thesis, Stevens Institute of Technology, 110 pp. [Available from Stevens Institute of Technology, 1 Castle Point, Hoboken, NJ 07030.]
- , J. Koskulics, K. Stamnes, B. Hamre, J. J. Stamnes, and R. P. Lawson, 2010: Optical properties of mixed phase boundary layer clouds observed from a tethered balloon platform in the Arctic. *J. Quant. Spectrosc. Radiat. Transfer*, **111**, 1921–1930.

- Stamnes, K., and R. Storvold, 1999: Development and deployment of a powered tethered balloon system at the SHEBA ice station for measurements of cloud micro-physical and radiative properties. *Proc. Ninth Atmospheric Radiation Measurement (ARM) Science Team Meeting*, San Antonio, TX, ARM, 7 pp. [Available online at http://www.arm.gov/publications/proceedings/conf09/extended_abs/stamnes_k.pdf.]
- , S.-C. Tsay, W. Wiscombe, and K. Jayaweera, 1988: Numerically stable algorithm for discrete-ordinate-method radiative transfer in multiple scattering and emitting layered media. *Appl. Opt.*, **27**, 2502–2509.
- Sun, Z., and K. Shine, 1994: Studies of the radiative properties of ice and mixed-phase clouds. *Quart. J. Roy. Meteor. Soc.*, **120**, 111–137.
- Tsay, S.-C., K. Stamnes, and K. Jayaweera, 1989: Radiative energy budget in the cloudy and hazy Arctic. *J. Atmos. Sci.*, **46**, 1002–1018.
- , —, and —, 1990: Radiative transfer in stratified atmospheres: Description and validation of a unified model. *J. Quant. Spectrosc. Radiat. Transfer*, **43**, 133–148.
- Verlinde, J., and Coauthors, 2007: The Mixed-Phase Arctic Cloud Experiment. *Bull. Amer. Meteor. Soc.*, **88**, 205–221.
- Walsh, J. E., and W. L. Chapman, 1998: Arctic cloud–radiation–temperature associations in observational data and atmospheric reanalyses. *J. Climate*, **11**, 3030–3045.
- Zhang, T., K. Stamnes, and S. A. Bowling, 1996: Impact of clouds on surface radiative fluxes and snowmelt in the Arctic and subarctic. *J. Climate*, **9**, 2110–2123.
- , S. A. Bowling, and K. Stamnes, 1997: Impact of the atmosphere on surface radiative fluxes and snowmelt in the Arctic and subarctic. *J. Geophys. Res.*, **102** (D4), 4287–4302.
- Zuidema, P., and Coauthors, 2004: An Arctic springtime mixed-phase cloudy boundary layer observed during SHEBA. *J. Atmos. Sci.*, **62**, 160–176.